LSPR enhanced MSM UV photodetectors

2012 Nanotechnology 23 444010

(http://iopscience.iop.org/0957-4484/23/44/444010)

Nanotechnology **23** (2012) 444010 (5pp) doi:10.1088/0957-4484/23/44/444010

LSPR enhanced MSM UV photodetectors

Serkan Butun[1,2], **Neval A Cinel**[1,3] **and Ekmel Ozbay**[1,2,3]

[1] Nanotechnology Research Center, Bilkent University, Bilkent, 06800 Ankara, Turkey
[2] Department of Physics, Bilkent University, 06800 Ankara, Turkey
[3] Department of Electric and Electronics Engineering, Bilkent University, 06800 Ankara, Turkey

E-mail: butun@bilkent.edu.tr

Received 8 March 2012, in final form 2 May 2012
Published 18 October 2012
Online at stacks.iop.org/Nano/23/444010

Abstract
We fabricated localized surface plasmon resonance enhanced UV photodetectors on MOCVD grown semi-insulating GaN. Plasmonic resonance in the UV region was attained using 36 nm diameter Al nanoparticles. Extinction spectra of the nanoparticles were measured through spectral transmission measurements. A resonant extinction peak around 300 nm was obtained with Al nanoparticles. These particles gave rise to enhanced absorption in GaN at 340 nm. Spectral responsivity measurements revealed an enhancement factor of 1.5. These results provided experimental verification for obtaining field enhancement by using Al nanoparticles on GaN.

(Some figures may appear in colour only in the online journal)

1. Introduction

Optoelectronic devices are getting smaller for better performance in terms of sensitivity, spatial resolution, high speed operation and technological developments [1]. Nano-scaled integrated circuit elements have gained much attention due to the demand from the market for flexible, faster and more responsive electronic components. The down side of this miniaturization of the individual circuit elements, however, is the reduction of the absorption cross section for photodetectors in particular. Furthermore, when the device size is shorter than the wavelength, diffraction limits the amount of detectable radiation [2–5].

The light is scattered by small metallic particles because of the resonant plasma oscillations of the conduction electrons. In a small particle, unlike infinite metal–dielectric interfaces, there is not enough space for surface plasmons to propagate. Instead there occurs a resonant mode depending on the size and shape of the particle. Localized surface plasmon resonance (LSPR) is a manifestation of SPs on nano-sized metallic particles. SPs interfere constructively at a resonance frequency depending on the size and the shape of the particle. Thus, a strong extinction is apparent in the transmission spectrum of the nanoparticles [6]. This extinction causes the localization of the electric field at the resonance frequency in the vicinity of the particle. This property has led to the use of metal nanoparticles in many applications such as surface enhanced Raman scattering [7–10] and biosensing [10–19]. There are also reports suggesting that this localized field can enhance the light absorption in the vicinity of the nanoparticles for thin film and organic photovoltaics [20–29].

UV monitoring has many potential civil and military applications. For instance *in situ* temperature monitoring in nuclear power plants and internal combustion engines, telecommunication (inter-satellite communication in particular), secure non-line-of-sight communication, ozone layer monitoring, biochemical agent detection, instrument calibration for UV lithography, missile plume detection etc [30, 31]. An optically small UV photodetector can further enhance the performance of conventional UV photodetectors. However, one must use a different metal which supports LSPR in UV rather than the commonly used metals such as Ag or Au. Al with its high bulk plasma frequency (15 eV) is a promising candidate for UV plasmonics.

Mie established a general theory to explain the scattering from gold nanoparticles which was later called after him as the Mie Theory. The polarizability in this theory for larger particles with sizes comparable to the wavelength of excitation can be written as [32, 33]

$$\alpha = \frac{1 - \frac{1}{10}(\varepsilon + \varepsilon_{\mathrm{m}})x^2 + o(x^4)}{\frac{1}{3} + \frac{\varepsilon_{\mathrm{m}}}{\varepsilon - \varepsilon_{\mathrm{m}}} - \frac{1}{30}(\varepsilon + 10\varepsilon_{\mathrm{m}})x^2 - \mathrm{i}\frac{4}{3}\pi^2\varepsilon_{\mathrm{m}}^{3/2}\frac{V}{\lambda} + O(x^4)}V \quad (1)$$

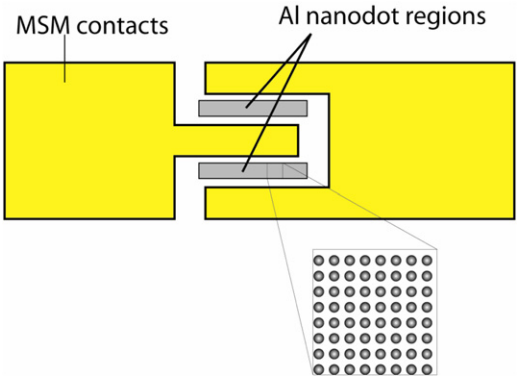

Figure 1. Conceptual drawing of an LSPR enhanced MSM photodetector (viewed from the top).

where V is the volume of the nanoparticle and $x = 2\pi r/\lambda$, the size parameter. The quadratic term in the numerator explains the retardation effect in excitation of the whole volume of the particle which shifts the resonance. The quadratic term in the denominator shifts the resonance further due to the retardation of the depolarization field. For Drude-like metals this shift in resonance is towards red as particle size increases. The dielectric permittivity of the metal, ε_m, plays a crucial role in this equation. Different metals exhibit resonances at different wavelengths even if their diameters are the same.

The quantitative analysis of the behavior of metallic nanoparticles requires rigorous calculations. Nevertheless, these formulations are limited to basic geometries such as spheres. Kuwata *et al* developed an analytical model for ellipsoid particles [32]; however, they establish their model based on experimental data. Because of analytical limitations, finite difference time domain (FDTD) simulations are often used to predict resonance behavior of a specific nanoparticle.

In this study, LSPR enhanced photodetectors on the GaN active layer operating in the UV regime are designed . The design consists of Al nanoparticles fabricated between the Schottky contacts of an MSM photodetector on a semi-insulating GaN active layer. A schematic drawing of the fabricated device is shown in figure 1. We fabricated Al nano-dots of 30 nm diameter and 100 nm period with e-beam lithography. We used Al because the plasma frequency of widely used metals such as Ag and Au is not sufficient to create a plasmonic response in the UV regime, which is required for the GaN platform. Bias voltage was kept low in order to collect the photo-generated carriers in the vicinity of the Schottky contacts. We were able to compare the effect of plasmonic particles on the quantum efficiency of the device.

2. Fabrication and results

The Al nanoparticles were fabricated using a Raith E-line e-beam lithography system. Single dot exposure was used and the diameter of the particles was varied by changing the dose of the exposure. Sapphire and GaN were used alternatively as substrates for the fabrication. The Al nanoparticles fabricated on sapphire were used for transmission measurements whereas those fabricated on GaN substrate were used as photodetectors. The details of the growth conditions of the GaN epitaxial layer can be found in our previous report [34]. We fabricated several samples with different particle diameters and periods. Diameters of the particles were varied between 20 and 60 nm in 5 nm steps while the period was varied from 100 to 200 nm in 25 nm steps. The total area covered with nanoparticles was $50 \times 50\ \mu m^2$.

We have designed and assembled a custom spectral micro-transmission setup for the extinction measurements of the fabricated Al nanoparticles (figure 2). The light from a broad spectrum Xe lamp (1) is carried to a collimating f-number matched UV lens (2) through a non-solarized UV multimode fiber. Then light is focused on the sample with the secondary lens (3). The sample is mounted on a special pcb board (x) and is placed on a micro-positioner for translation. After passing through the sample, the light is collected with the imaging lens (4). The image is projected on to a plane where there is placed a variable aperture (5). This aperture allows us to select the area where a transmission measurement is desired. Light is then folded by an easy mount mirror (6) towards camera focusing optics (7). We monitor the position of the samples with a CCD camera (8). We remove the folding mirror after the individual nanoparticle area is aligned and selected with the aperture. Another focusing lens (9) couples the light to the collection fiber. The spectrum is then measured by an Oceanoptics USB4000 model spectrometer (10).

Figure 3 illustrates the fabricated Al nanoparticles and the spectral transmission response of the structure. The size distribution suggests a very uniform fabrication. Here we present two selected extinction spectra of Al nanoparticles at two different wavelengths. The resonance shifts towards red as the diameter of the particle increases as expected. In addition resonance gets stronger as the diameter increases because particles become more closely packed, which increases the inter-coupling between the particles. We performed FDTD simulations for further justification of the measurements using a commercial software package by Lumerical Inc. Our simulations are in excellent agreement with the measured values. It should be noted that these are fabricated on sapphire which has a refractive index of 1.8. Actual devices are fabricated on GaN nitride which has a much higher refractive index ($\sim$2.5). This will cause a red-shift in the resonant wavelength. We expect the peak resonance will be at 339 for 36 nm diameter particles when they are fabricated on GaN. Here we assumed that the effect of substrate on the effective refractive index of the surrounding environment is limited by the bottom area of the nanoparticle.

The calculated electric field (E-field) distributions in the vicinity of the Al nanoparticles are illustrated in figure 4. Here we compare the E-field intensities at different wavelengths. When the wavelength of illumination is near the LSPR peak, there is a strong confinement in the dielectric compared to an illumination wavelength which is far from the resonance. This further explains the enhanced absorption in the semiconductor. Note that, we could not repeat FDTD simulations of Al nanoparticles on GaN substrates since our simulation tool does not provide a reasonable material fitting for the real and complex parts of the dielectric function of GaN in order to calculate its absorption.

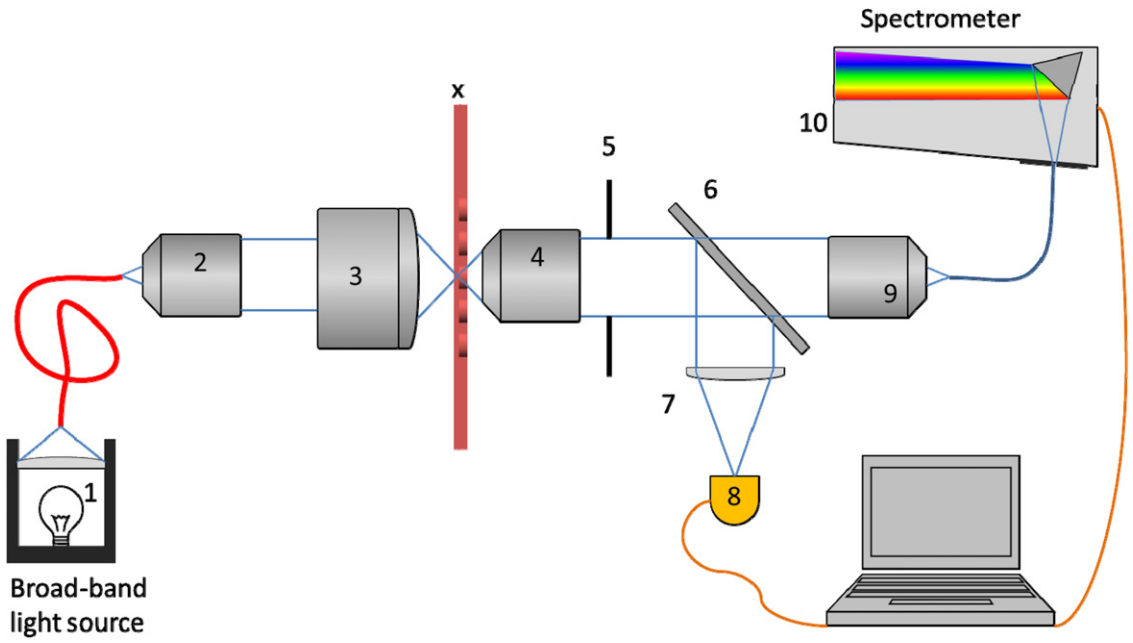

Figure 2. Schematic of the micro-transmission setup.

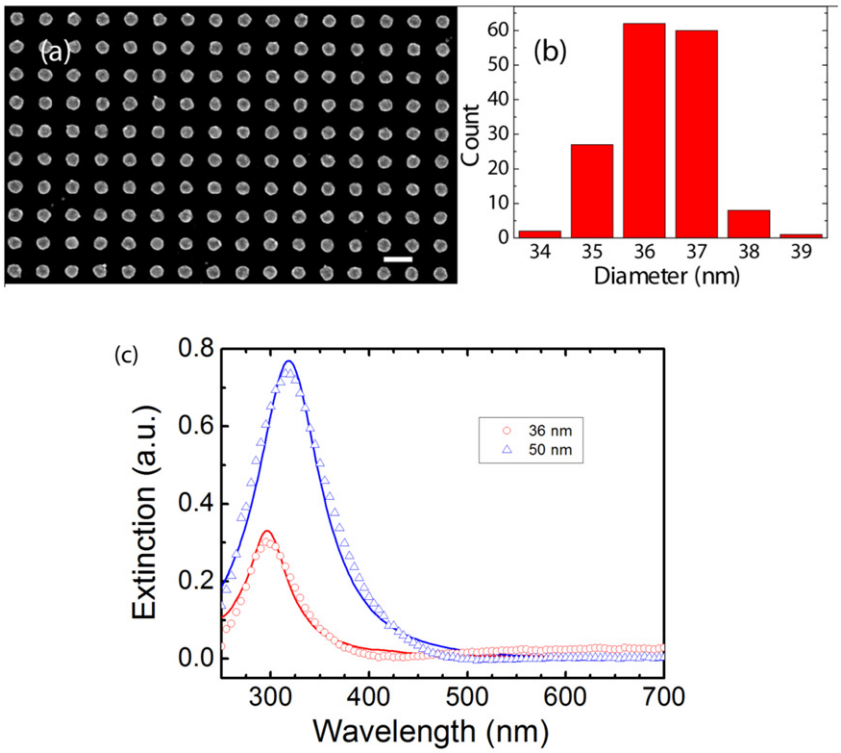

Figure 3. Fabricated Al nanoparticles: (a) a scanning electron microscopy image of the particles. Scale bar is 100 nm. (b) Size distribution of the particles in the image in (a). (c) The extinction spectra of the Al nanoparticles with two different diameters fabricated on sapphire. Dots represent the measurements whereas lines correspond to FDTD simulations.

The fabrication of the MSM photodetectors started with Schottky contact metallization with optical lithography. The contact distance was 20 μm. We used Ni/Au as contact metal. The design includes large probing pads. Therefore this was a single-step process. Then we fabricated Al nanoparticles with 36 nm diameter and 100 nm in period with e-beam lithography. The size and the period of the particles were then confirmed with scanning electron microscopy (SEM). We fabricated photodetectors without nanoparticles as reference devices as well.

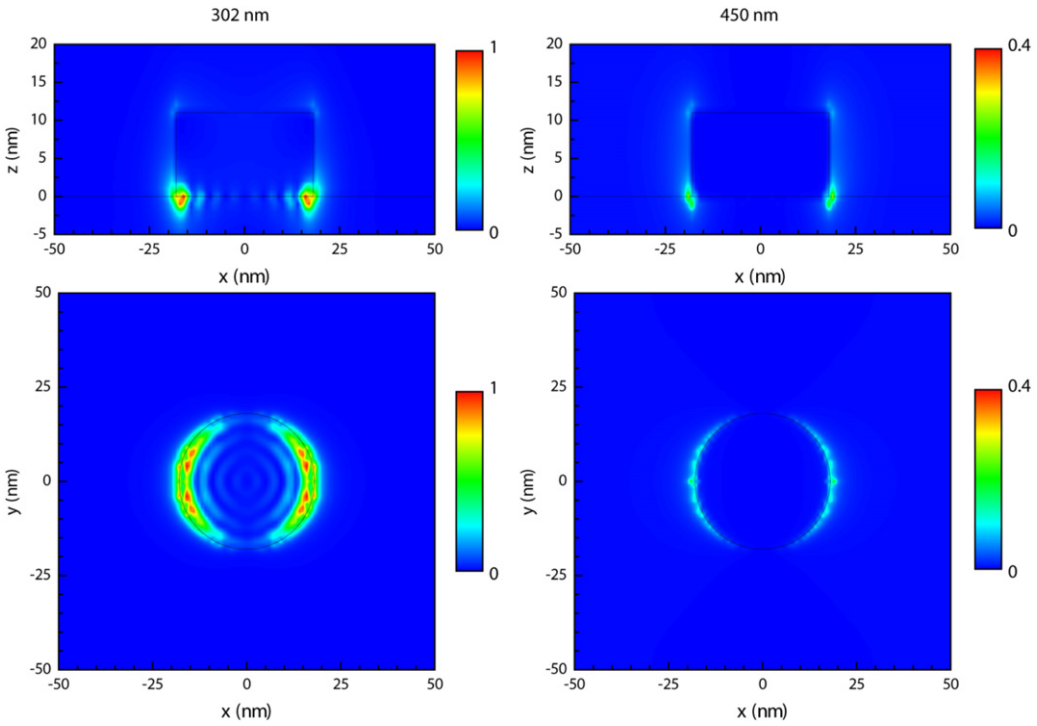

Figure 4. E-field intensity distributions of the Al nanoparticles on sapphire substrate calculated via FDTD simulations. On the left, normalized (to the maximum value) E-field intensity distribution cross sections at a resonant wavelength of 302 nm are shown. Whereas, distributions at an off resonant wavelength of 450 nm are presented on the right for comparison. The z direction is normal to the surface and the sapphire/air interface lies within the $z = 0$ plane.

We measured spectral responsivity characteristics of the LSPR enhanced photodetectors using a Stanford Research Systems SR830 Lock-in Amplifier. The output of the UV enhanced Xe lamp (Spectral Products ASB-XE-175) was monochromated (Spectral Products DK240) then modulated mechanically by a chopper. It is then coupled to a multimode non-solarized UV enhanced 100 μm diameter fiber which was used to illuminate the photodetector under test. We calibrated the spectral output power illumination setup with a NIST-traced calibrated Si photodetector (Newport 818-UV-L). We measured both photodetectors with nanoparticles and without nanoparticles. The results are illustrated in figure 5 in a comparative manner and they reveal a significant increase in the quantum efficiency around 340 nm. We analyzed these results further in order to calculate the enhancement. figure 6 shows that we have almost 50% enhancement in the quantum efficiency which is due to the localization of the incident electromagnetic field on the surface where most of the light is collected in an MSM photodetector. Here we cut the curve at 360 nm simply because the data at longer wavelengths have no meaning since GaN is completely transparent in that region.

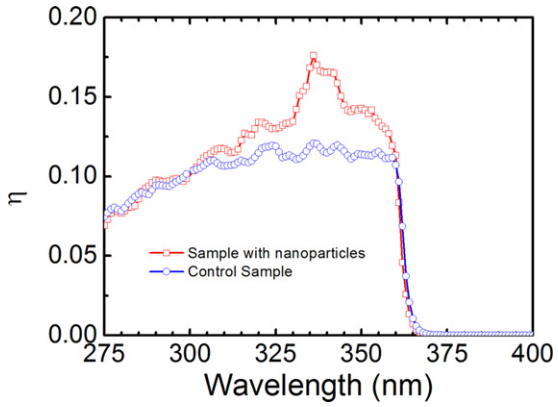

Figure 5. Spectral quantum efficiency measurement of the LSPR enhanced photodetector along with the control sample.

3. Conclusion

In conclusion, we examined the effects of plasmonic scattering on absorption and photocurrent collection in the prototype visible blind GaN photodetector with size-optimized Al nanoparticles. At wavelengths of surface plasmon resonance, scattered incident light by the nanoparticles yielded enhanced absorption in the active layer of the photodetector. Al nanoparticles were first investigated separately via spectral transmission measurements. An enhancement of 50% at 340 nm was measured in the fabricated photodetector. The results showed that scattering with nanoparticles enhances the absorption in the UV region. This enhancement can increase the detectivity performance of a photodetector.

Acknowledgments

This work is supported by the projects DPT-HAMIT, ESF-EPIGRAT, EU-N4E, NATO-SET-181 and TUBITAK

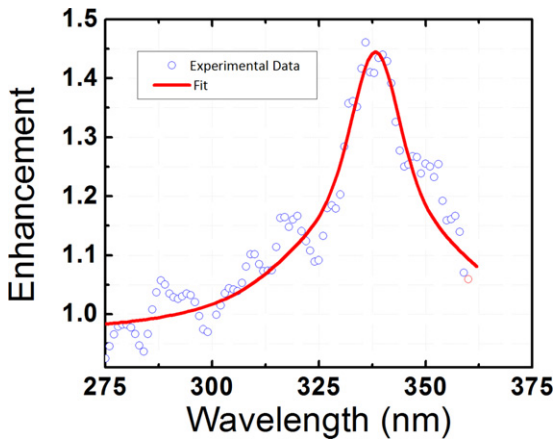

Figure 6. Enhancement of the quantum efficiency with Al nanoparticles.

under Project Nos, 107A004, 107A012, 109E301. One of the authors (EO) also acknowledges partial support from the Turkish Academy of Sciences.

References

[1] Ozbay E 2006 Plasmonics: merging photonics and electronics at nanoscale dimensions *Science* **311** 189–93
[2] Goodman J W, Leonberger F J, Kung S Y and Athale R A 1984 Optical interconnections for VLSI systems *Proc. IEEE* **72** 850–66
[3] Krishnamoorthy A V and Miller D A B 1996 Scaling optoelectronic-VLSI circuits into the 21st century: a technology roadmap *IEEE J. Sel. Top. Quantum Electron.* **2** 55–76
[4] Meindl J D, Davis J A, Zarkesh-Ha P, Patel C S, Martin K P and Kohl P A 2002 Interconnect opportunities for gigascale integration *IBM J. Res. Dev.* **46** 245–63
[5] Miller D A B 2000 Rationale and challenges for optical interconnects to electronic chips *Proc. IEEE* **88** 728–49
[6] Willets K A and Van Duyne R P 2007 Localized surface plasmon resonance spectroscopy and sensing *Annu. Rev. Phys. Chem.* **58** 267–97
[7] Hossain M K, Kitahama Y, Huang G G, Han X X and Ozaki Y 2009 Surface-enhanced Raman scattering realization of localized surface plasmon resonance using unique substrates and methods *Anal. Bioanal. Chem.* **394** 1747–60
[8] Masson J F, Murray-Methot M P and Live L S 2010 Nanohole arrays in chemical analysis manufacturing methods and applications *Analyst* **135** 1483–9
[9] Pieczonka N P W and Aroca R F 2008 Single molecule analysis by surfaced-enhanced Raman scattering *Chem. Soc. Rev.* **37** 946–54
[10] Willets K A and Van Duyne R P 2007 Localized surface plasmon resonance spectroscopy and sensing *Annu. Rev. Phys. Chem.* 267–97
[11] Anker J N, Hall W P, Lyandres O, Shah N C, Zhao J and Van Duyne R P 2008 Biosensing with plasmonic nanosensors *Nature Mater.* **7** 442–53
[12] Haes A J, Stuart D A, Nie S M and Van Duyne R P 2004 Using solution-phase nanoparticles, surface-confined nanoparticle arrays and single nanoparticles as biological sensing platforms *J. Fluoresc.* **14** 355–67
[13] Haes A J and Van Duyne R P 2004 A unified view of propagating and localized surface plasmon resonance biosensors *Anal. Bioanal. Chem.* **379** 920–30
[14] Hutter E and Fendler J H 2004 Exploitation of localized surface plasmon resonance *Adv. Mater.* **16** 1685–706
[15] Jain P K, Huang X H, El-Sayed I H and El-Sayed M A 2008 Noble metals on the nanoscale optical and photothermal properties and some applications in imaging, sensing, biology, and medicine *Acc. Chem. Res.* **41** 1578–86
[16] Mannelli I and Marco M P 2010 Recent advances in analytical and bioanalysis applications of noble metal nanorods *Anal. Bioanal. Chem.* **398** 2451–69
[17] Sepulveda B, Angelome P C, Lechuga L M and Liz-Marzan L M 2009 LSPR-based nanobiosensors *Nano Today* **4** 244–51
[18] Zhang X Y, Whitney A V, Zhao J, Hicks E M and Van Duyne R P 2006 Advances in contemporary nanosphere lithographic techniques *J. Nanosci. Nanotechnol.* **6** 1920–34
[19] Zhao J, Zhang X Y, Yonzon C R, Haes A J and Van Duyne R P 2006 Localized surface plasmon resonance biosensors *Nanomedicine* **1** 219–28
[20] Atwater H A and Polman A 2010 Plasmonics for improved photovoltaic devices *Nature Mater.* **9** 205–13
[21] Catchpole K R and Polman A 2008 Plasmonic solar cells *Opt. Express* **16** 21793–800
[22] Catchpole K R and Polman A 2008 Design principles for particle plasmon enhanced solar cells *Appl. Phys. Lett.* **93** 191113
[23] Derkacs D, Lim S H, Matheu P, Mar W and Yu E T 2006 Improved performance of amorphous silicon solar cells via scattering from surface plasmon polaritons in nearby metallic nanoparticles *Appl. Phys. Lett.* **89** 093103
[24] Ferry V E, Sweatlock L A, Pacifici D and Atwater H A 2008 Plasmonic nanostructure design for efficient light coupling into solar cells *Nano Lett.* **8** 4391–7
[25] Konstantatos G and Sargent E H 2010 Nanostructured materials for photon detection *Nature Nanotechnol.* **5** 391–400
[26] Morfa A J, Rowlen K L, Reilly T H, Romero M J and van de Lagemaat J 2008 Plasmon-enhanced solar energy conversion in organic bulk heterojunction photovoltaics *Appl. Phys. Lett.* **92** 013504
[27] Nakayama K, Tanabe K and Atwater H A 2008 Plasmonic nanoparticle enhanced light absorption in GaAs solar cells *Appl. Phys. Lett.* **93** 121904
[28] Pillai S, Catchpole K R, Trupke T and Green M A 2007 Surface plasmon enhanced silicon solar cells *J. Appl. Phys.* **101** 093105
[29] Westphalen M, Kreibig U, Rostalski J, Luth H and Meissner D 2000 Metal cluster enhanced organic solar cells *Sol. Energy Mater. Sol. Cells* **61** 97–105
[30] Morkoc H, Strite S, Gao G B, Lin M E, Sverdlov B and Burns M 1994 Large-band-gap SiC, III–V nitride, and II–VI ZnSn-based semiconductor-device technologies *J. Appl. Phys.* **76** 1363–98
[31] Mohammad S N, Salvador A A and Morkoc H 1995 Emerging gallium nitride based devices *Proc. IEEE* **83** 1306–55
[32] Kuwata H, Tamaru H, Esumi K and Miyano K 2003 Resonant light scattering from metal nanoparticles practical analysis beyond Rayleigh approximation *Appl. Phys. Lett.* **83** 4625–7
[33] Meier M and Wokaun A 1983 Enhanced fields on large metal particles dynamic depolarization *Opt Lett.* **8** 581–3
[34] Butun S, Gokkavas M, Yu H B and Ozbay E 2006 Low dark current metal–semiconductor–metal photodiodes based on semi-insulating GaN *Appl. Phys. Lett.* **89** 073503